PHYSICAL REVIEW B **70**, 195203 (2004)

Modeling of the structure and properties of oxygen vacancies in amorphous silica

Sanghamitra Mukhopadhyay,* Peter V. Sushko, A. Marshall Stoneham, and Alexander L. Shluger†
Department of Physics and Astronomy, University College London, London WC1E 6BT, United Kingdom

(Received 12 May 2004; published 9 November 2004)

We used an embedded cluster method to predict and characterize possible structural types of neutral and positively charged oxygen vacancies in amorphous silica. Defects were treated at 70 different oxygen sites of continuous random network amorphous structure generated using classical molecular dynamics. The neutral vacancies are characterized by a wide distribution of formation energies and structural parameters. Our modeling predicts the two major structural types of positively charged vacancies (E' centers): dimer and dangling bond centers. The local structure of both types of centers depends on the medium range structure of the surrounding amorphous network. The majority of the dangling bond centers are unpuckered. We used structural "fingerprints" derived from similar calculations of oxygen vacancy type centers in quartz and from experiment to find two other structural types of dangling bond centers: the puckered configuration and the back-projected configuration of E' centers. In each case we find a distribution of both structural and EPR parameters. However, the average values of the EPR parameters for all dangling bond configurations are very similar. The structural criteria which favor the formation of different types of centers in the original amorphous structure are formulated in terms of the average Si-O distance of oxygen ion with its two neighboring silicon ions.

DOI: 10.1103/PhysRevB.70.195203 PACS number(s): 61.72.Ji, 61.72.Bb, 61.43.Fs, 61.80.Az

I. INTRODUCTION

Theoretical modeling of effects of structural disorder on defect properties and relative abundance of different defect configurations in amorphous materials is only starting to develop, in spite of a long history of defect studies. In this paper, we consider oxygen vacancies in amorphous silica, a-SiO$_2$, which, due to its broad technological applications, is one of the most studied materials.[1,2] We develop a consistent approach to predicting and analyzing defect structures in amorphous materials and use it to resolve some of the controversies pertaining to the structure and relative abundance of positively charged oxygen vacancies in a-SiO$_2$.

Amorphous silica is a generic name for a wide range of materials used in the cores of optical fibers and in most silicon-based metal-oxide-semiconductor devices. Theory deals, however, with some idealized models of amorphous structure and mechanisms of defect formation. A common model of amorphous silica is that of continuum random network where the crystalline connectivity is preserved and the geometric parameters are distributed in certain ranges.[3] One then expects that defects would look similar to their analogues in the crystalline structure, again with distributed parameters. Already at this simplified level, modeling defects in amorphous materials requires considering not one or several sites, as in crystals, but a statistical ensemble of structural sites. Indeed, the recent theoretical studies of peroxy linkage species[4] and of interstitial oxygen molecules[5] demonstrate that the structures of these defects in quartz and in amorphous silica are very similar. However, the formation energies, structural parameters, diffusion barriers and spectroscopic parameters depend on details of the local and medium-range environment and can be characterized by some distributions.

The family of positively charged oxygen vacancies, known as E' centers, in crystalline and amorphous SiO$_2$ provides yet another set of examples. In a series of works Weeks and Nelson,[6] Silsbee,[7] and Jani *et al.*[8] measured with very high precision all the strong and weak hyperfine interactions, including directions for the principal values of the E'_1 center in α quartz. The prevailing model of this defect, pioneered by Rudra and Fowler[9] is shown in Fig. 1(a). It is considered to be a positively charged oxygen vacancy which adopts a so- called puckered configuration (PC). Here the Si$_S$ accommodates an unpaired electron on a dangling bond whereas the silicon Si$_L$ relaxes through the plane of its three neighboring oxygen atoms and forms a bond with an oxygen O$_B$ in Fig. 1(a). Allan and Teter were the first to demonstrate that along with the PC there is the dimer configuration (DC) [see Fig. 1(b)], wherein the two silicon atoms that face the vacancy relax very little away from their ideal positions in the perfect quartz lattice.[10] Most calculations predict PC to be lower in energy than DC[11] and there is no clear experimental evidence that DC is significantly populated in α quartz.

Contrary to α quartz, several atomistic models have been proposed for E' centers detected in amorphous silica mainly using EPR.[12–14] E' center is now understood in a more general sense as rather a $\cdot$Si$\equiv$O$_3$ silicon dangling bond with an unpaired electron, which can exist on its own as a neutral defect, as a part of a positively charged oxygen vacancy (as in Fig. 1), or as an even more complex defect. These defects are labeled by subscripts α, β, γ, δ to distinguish species characterized by different EPR parameters (see, for example, Ref. 12). However, their structural models are still controversial. For example, there are at least four different models of E'_δ centers.[15–18] The existence of topologically different E'_γ centers in γ-irradiated silica has recently been suggested on the basis of the analysis of fine features in the EPR spectra.[19,20] Several more models of paramagnetic "oxygen deficient" and "silicon dangling bond" centers have been proposed in theoretical simulations.[17,21–25] Experimentally, EPR signals attributed to different centers are shown to coexist in some of the samples.[12] However, relative concentrations of different centers depend on the sample preparation,

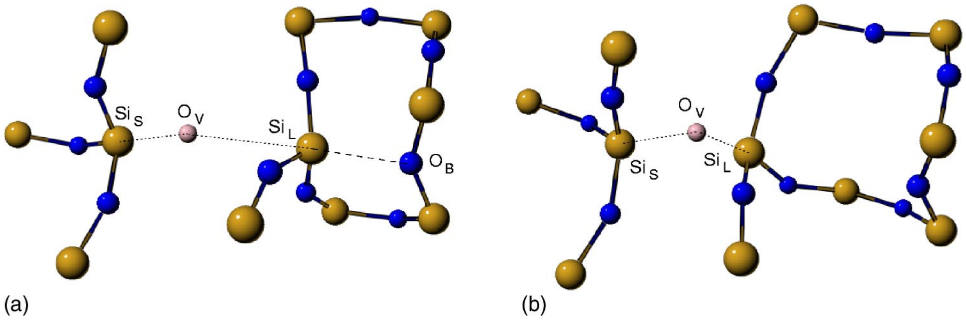

FIG. 1. (Color online) Two configurations of the E_1' center in α quartz: (a) puckered configuration and (b) dimer configuration. In (a) Si_L (Si atom of the longer Si-O bond) is puckered and makes a bond with an oxygen ion (O_B), Si_S (Si of the shorter Si-O bond) carries the unpaired electron. O_V marks the oxygen vacancy site.

presence of impurities (e.g., H, F, Cl, P) and method of irradiation (e.g., photons, electrons, high energy ions[26,27] and neutrons[28]).

One way to understanding the origins of different defect configurations in amorphous materials, such as E' centers, and predicting their relative concentrations is to correlate the local structural characteristics of oxygen sites in amorphous material—bond lengths, ring size, dihedral angles—with structural models and properties of defects created at these sites. This is relatively straightforward using theoretical tools: one should build a model of an amorphous structure and then produce defects in a selection of sites and build a distribution of defect parameters. This approach has been used to study peroxy linkage defects[4] and oxygen diffusion,[5] and recently to analyze different types of E' centers in silica.[23,29,30] This approach proves to be very illuminating, but does not allow one to build good statistics if small periodic cells of amorphous structure are used.

Another approach has been to transfer defect models developed in a crystalline phase into amorphous phase. In particular, the model of the E_1' center developed for α quartz has been considered to be a natural prototype of the E_γ' center in a-SiO$_2$. Following this approach, one needs to search for local regions in an amorphous structure which can accommodate the most stable "puckered" configuration of the E_1' center in quartz. This requires having a "back oxygen" in the appropriate position to stabilize the puckering Si ion [see Fig. 1(a)]. To find all such sites in the amorphous structure one should describe the PC in terms of structural parameters characterizing the position of the back oxygen with respect to the vacancy site. Two similar sets of such "fingerprints" have been proposed and tested in Refs. 23 and 30 on the basis of calculated models of E' centers in a-SiO$_2$ and in α quartz.

On the experimental front, several studies analyzed the line shape of EPR signals attributed to E' centers in different silica samples.[19,20,31] In particular, Griscom and Cook[20] focused on the question whether the ^{29}Si hyperfine interaction of the E' center could be used as a probe of the intermediate range order in silica glass. Employing the computer line-shape simulation methods they came up with a hypothesis that most of the E' centers in the glass samples they examined existed in backward projected dangling bond configuration similar to the model of E_2' centers discussed by Feigl *et al.*[32] Only a small proportion of E' centers in these samples would exist in the "classical" forward projected dangling bond configuration. However, it is impossible to say whether this would result from the local glass structure, is induced by the defect or in the process of its generation. Further, Griscom and Cook[20] proposed a set of "fingerprints" for the backward projected configuration of the E_γ' center. However, they have not been tested by theoretical modeling.

In this paper we attempt to *predict* possible structural types of E' centers in amorphous silica using a specific model of their creation via hole trapping by neutral vacancies.

First, we generate a representative model of amorphous structure. Then we use an embedded cluster method to study the structure and properties of neutral oxygen vacancies formed at about 70 different sites. We then consider defects formed by ionizing these neutral vacancies. In this way we create a distribution of centers with structures ranging from a dimer to a dangling bond configuration. This, however, does not exhaust all possible structures of E' centers in amorphous silica. We then explore a "fingerprint" approach: using the E_1' center model calculated in crystalline quartz and the criteria proposed from the analysis of EPR by Griscom and Cook,[20] we search for local regions in an amorphous structure, which match these descriptions. In this way we find the puckered and back-projected configurations and discuss their stability. We verify our findings by comparing the calculated hyperfine (hf) and superhyperfine (shf) EPR parameters with the experimental data. In the Appendix we discuss the dependence of the results on the method of calculation and demonstrate that the character of localization of an unpaired electron in positively charged oxygen vacancies depends on the amount of exact exchange contribution in a density functional employed.

The main new results of this work can be summarized as follows. (i) We find that, similar to the peroxy linkage defect,[4] neutral oxygen vacancies in different sites of an amorphous structure are qualitatively similar, and can be characterized by a wide distribution of formation energies and structural parameters. (ii) The structure of positively charged vacancies is determined by the structure of the precursor neutral vacancies: they may form dimer, dangling bond with an unpuckered second silicon ion, dangling bond with a puckered second silicon ion, and back-projected dangling bond configurations (see schematics in Fig. 7). (iii) In each case we find a distribution of both structural and EPR parameters. However, the average values of the EPR parameters for all dangling bond configurations are very close. (iv) The expected concentration of dimers is much smaller than that of dangling bond configurations with an unpuckered second silicon ion. The number of sites capable of accommodating puckered dangling bond configurations of positively charged oxygen vacancy in the ideal amorphous network is predicted to be about 10%. We conclude that, unlike the E_1' center in α quartz, puckering of the silicon ion bearing a hole is not the necessary feature of E_γ' center structure in amorphous silica. Moreover, the most likely structure of positively charged oxygen vacancies in a-SiO$_2$ is a dangling bond on one silicon and the unpuckered second silicon ion of the vacancy.

In the next section we discuss the methods of calculations. The results of our modeling are described in Sec. III and discussion is in Sec. IV.

II. METHODS OF CALCULATIONS

Most of the calculations dealing with defects in amorphous silica so far have been made using either periodic or molecular cluster models. In the periodic model, the disorder of the amorphous structure is included explicitly, but within a relatively small periodically translated unit cell. Most of the quantum mechanical calculations of defects in a-SiO$_2$ previously carried out in this model were confined to unit cells of less than 100 atoms. Thus the number of defect sites available for statistical analysis has been very limited. On the other hand, in the molecular cluster model, one can capture at best only the average atomic structure of the a-SiO$_2$. Besides, these clusters typically include only 10–50 atoms which is hardly enough to reproduce even the medium-range structural deformation induced by the defect. A problem pertaining to both models has been the dependence of the results on the quantum mechanical method (see, for example, Refs. 33 and 34). In particular, as has been demonstrated in Ref. 35, there can be a dramatic change in the defect electronic structure depending on whether Hartree-Fock or density functional theory (DFT) were used.

Our approach is based on the implementation of an embedded cluster method. We first generate a relatively large model of silica structure using classical molecular dynamics and then calculate defects and their properties for a number of selected sites within that structure using the embedded cluster method.[36] This method has been used successfully to study defects in ionic crystals[37–40] and its applicability to modeling defects in α quartz has been demonstrated in recent publications.[30,33,34]

In the following we describe the embedded cluster approach and the details of the preparation and characterization of the a-SiO$_2$ structure.

A. Preparation and characterization of the amorphous structure

The amorphous SiO$_2$ structure used in this work was generated using the molecular Dynamics (MD) method, classical interatomic potentials and periodic supercells. We followed an earlier work by Vollmayr *et al.*[41] with several changes summarized below.

TABLE I. Parameters of the classical interatomic interaction V_d with damped van der Waals term.

Parameters		Interaction O-O	Interaction Si-O
r_0	Å	1.9	1.18
B	eV	313.9554	505.0553
β	Å^{-1}	2.3502	3.5330

We use the DL_POLY code[42] and the Buckingham-type interatomic potentials developed by van Beest *et al.*[43] (BKS). The Buckingham-type potentials contain the dispersion term of $-1/r^6$ (where r is the distance between two atoms) and diverge at small interatomic distances. Therefore the BKS potentials were modified so that to avoid this unphysical behavior. In particular, we defined a new set of potentials as

$$V(r) = \begin{cases} V_{\mathrm{BKS}}(r) = Ae^{-\alpha r} - \dfrac{C}{r^6} & \text{if } r \geqslant r_0, \\ V_d(r) = Be^{-\beta r} & \text{if } r \leqslant r_0, \end{cases}$$

and derived positive parameters B and β from conditions

$$V_{\mathrm{BKS}}(r_0) = V_d(r_0),$$

$$V'_{\mathrm{BKS}}(r_0) = V'_d(r_0).$$

The matching point r_0 in the above equations was selected so that to minimize the deviation of $V(r)$ from $V_{\mathrm{BKS}}(r)$ in the physically meaningful region of r. The values of parameters B, β, and r_0 are given in Table I.

To generate an amorphous structure, we first defined a $2 \times 2 \times 2$ extension of the 24-atom β-crystoballite unit cell and then subjected it to melting, equilibration at high temperature and quenching to low temperature using the molecular dynamics technique and NPT ensemble. The simulation cell contained 648 atoms and was first heated to 7000 K at a rate of 5×10^{13} K/s (500 K per 10 ps), then equilibrated at 7000 K for 100 ps and finally quenched to 0 K at a rate of 8×10^{12} K/s (50 K per 6 ps). The final configuration of the a-SiO$_2$ structure was further relaxed using static calculations. The results obtained by Vollmayr *et al.*[41] suggest that slower quenching would not change the average structural properties of the a-SiO$_2$ structure.

The resulting a-SiO$_2$ model proves to be a continuous random network with all Si ions coordinated by four oxygen ions and all O ions coordinated by two silicon ions. It has the density of 2.37 g/cm^3, which is higher than the average density of 2.20 g/cm^3 usually attributed to amorphous silica.[44] This reflects the properties of the BKS potentials since the volume of the simulation cell was not fixed during the MD calculations. The distribution of Si-O nearest neighbor distances is given in Fig. 2(a) together with the distribution of Si-O-Si angles [Fig. 2(b)]. These distributions agree well

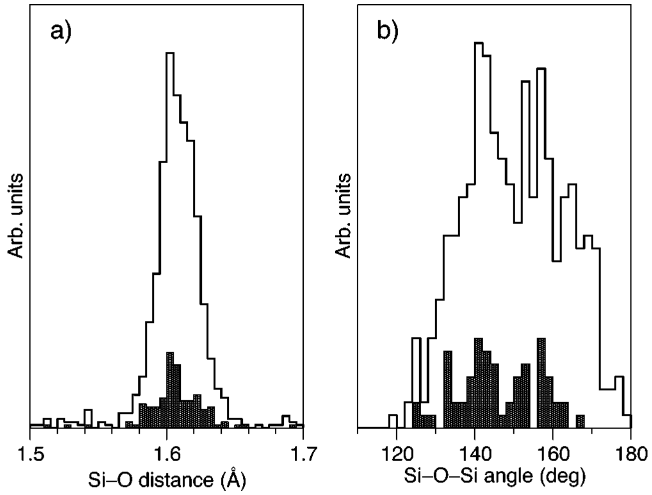

FIG. 2. Distributions of (a) Si-O distances and (b) Si-O-Si angles in MD 648-atom a-SiO$_2$ structures. The filled parts show the same distributions for the subset of sites chosen for the embedded cluster calculations.

with the previously reported in the literature.[1] The structure contains four three-member rings and 10 four-member rings with the maximum of the ring-size distribution corresponding to five- and six-member rings.

B. The embedded cluster method

The electronic structure of a-SiO$_2$ and that of defect centers was calculated using an embedded cluster technique implemented in the GUESS computer code.[36] The method is designed for studying point defects in polar solids and combines an *ab initio* quantum mechanical treatment of a “site of interest” and its surroundings with a classical description of the rest of the solid. It accounts for the electrostatic potential of the whole solid in the defect region and includes, consistently, both ionic and electronic contributions to the defect-induced polarization of the host lattice as well as the effect of the polarized lattice on the defect. The method and its applications to defects in the bulk of crystalline materials (including α quartz) and at low-coordinated surface sites have been thoroughly described in several recent publications.[33,34,36,38] Therefore we will only briefly outline the main features of the method and will focus on the details relevant to studying defects in a-SiO$_2$.

In broad terms, in the embedded cluster method a system, crystalline or amorphous, with a single point defect is divided into several regions. A spherical region I centered at the “site of interest” includes (i) a quantum-mechanically treated cluster (QM cluster), (ii) an interface region which connects the QM cluster and the rest of the solid treated classically, and (iii) a classical region that surrounds the QM cluster and includes up to several hundred atoms. Region I is surrounded by a finite region II, also treated atomistically and containing up to several thousand atoms. In the course of calculations, all positions of atoms within region I are fully optimized while atoms in region II remain fixed in the positions corresponding to a perfect crystalline or amorphous structure. Their purpose is to provide a correct electrostatic potential in region I and proper boundary conditions for the atoms at the border of regions I and II. Regions I and II combined together form a finite region which has a radius of several nanometers and is called nanocluster. Finally, to account for the polarization of the solid from the border between regions I and II and up to infinity, we introduce region III. It is treated in the approximation of polarizable continuum and conforms geometrically to the boundary between regions I and II.

The whole approach is similar in spirit to the classical Mott-Littleton method.[45] The total energy of the system includes (i) the energy of the QM cluster and the interface atoms in the external electrostatic potentials due to the classical environment; (ii) the interaction between classical atoms in regions I and II calculated using interatomic potentials; (iii) the short-range interaction of the classical atoms and of the interface atoms with the QM cluster atoms calculated using the short-range part of the classical interatomic potentials, and (iv) the Mott-Littleton correction for the polarization of region III. This latter correction is about 0.3 eV in the typical setup described below and remains constant in all calculations of singly charged vacancies. The expression for the total energy is given in Ref. 33.

The classical atoms in regions I and II are represented using the shell model and the rigid atom model, respectively. Their electrostatic interaction with the interface and with the QM cluster atoms is included on the quantum-mechanical level, i.e., by calculating the corresponding matrix elements and adding them to the QM potential energy matrix. Total forces are calculated on both QM and classical ions. This allows us to minimize the system total energy simultaneously with respect to the electronic coordinates and the positions of QM ions and classical ions, and hence to avoid the time consuming “self-consistency” procedure used in some previous implementations of this method.[46,47]

Properties of the interface atoms depend on material in question, as described for MgO,[36] SiO$_2$,[33] and Mg$_2$SiO$_4$.[38] For SiO$_2$, a QM cluster is terminated by the Si* atoms that form an interface between the QM cluster and the rest of the nanocluster. The Si* atoms are located at the Si sites of the SiO$_2$ structure and represent real Si atoms. This is quite different from many molecular cluster schemes where a QM cluster is terminated by artificial so-called pseudoatoms.[21,48,49] The Si* atoms are chosen so that they are coordinated by one quantum-mechanically treated oxygen and three classically treated oxygen ions from the rest of the nanocluster. They perform a dual role: they form a polar bond with the QM oxygen and describe the interaction with the three classical oxygens. This is achieved by representing Si* as a combination of $\frac{1}{4}$ of a quantum-mechanical Si atom and $\frac{3}{4}$ of a classical Si atom. The detailed description of Si* atoms as applied to α quartz is given in Refs. 33 and 34. The same parametrization scheme is used in the present calculations.

The GUESS code[33,36] plays the role of a “master” program that calculates the total energy, total forces acting on all centers in region I and performs the geometry optimization of the whole system. Thus the scheme allows us to account consistently for the defect-induced polarization of the host lattice and also the effect of this polarization on the defect itself. The GAUSSIAN 98 package[50] is used for calculations of the quantum mechanical contributions to the total energy and forces.

1. Building a finite region I+II

Defects formed at different sites of a disordered system can have entirely different properties or structures altogether. To build statistics, one must consider defects in many sites. Since in the embedded cluster method region I+II should be centered on the defect site, this implies that separate, generally nonequivalent, regions I+II or a nanoclusters must be built for each defect site. Further, the local atomic structure near each site of interest is unique, so QM clusters defined at these sites may have different topologies.

A nanocluster can be built in several different ways and may have different shapes. One of the possibilities is to build a nanocluster as an $n \times m \times l$ extension of a crystal unit cell or, in the case of amorphous SiO_2, of the 648-atom periodic simulation cell described above. However, we found that the electrostatic potential inside region I converges faster if $Si(\frac{1}{2}O)_4$ tetrahedra are used as "building blocks." This is because the $Si(\frac{1}{2}O)_4$ unit is not only neutral but also has a very small dipole moment and the dipole moments associated with these units in amorphous SiO_2 approximately cancel each other. The full cancellation is achieved in the α-quartz structure. We have found that if in α quartz a spherical nanocluster built from $Si(\frac{1}{2}O)_4$ units has the radius of about 30 Å and the radius of region I is about 13 Å, the deviation of the on-site electrostatic potential on different sites in region I does not exceed 0.01 eV. This deviation due to the finite size of the nanocluster decreases further with the increase of the nanocluster radius. It is of the same order of magnitude for a-SiO_2 with the same size of the nanocluster and region I. This deviation is also much smaller than the site-to-site variations of the potential induced by the structural disorder in a-SiO_2.

We note that regions I+II centered at different atoms of the a-SiO_2 unit cell differ in several respects. First, the total number of atoms in different nanoclusters is different. Second, since region I is defined only by its radius, the total number of atoms in region I will vary from one nanocluster to another. Finally, each nanocluster has a small dipole moment associated with it due to the incomplete cancellation of dipole moments associated with each $Si(\frac{1}{2}O)_4$ "building block." This will introduce an additional error in the on-site electrostatic potential inside the nanocluster. The effect of these factors is, however, small and can be neglected in analysis of the results.

2. Choosing QM clusters and basis sets

Two groups of QM clusters were used in these calculations. "Small" QM clusters comprise two neighboring corner-sharing tetrahedra: $Si_2O_7Si_6^*$, where Si* represent the interface atoms at the border of the QM cluster. The vacancy is then formed at the site of the shared oxygen atom. In the case of the three-member rings, the smallest clusters were either $Si_3O_9Si_6^*$ or $Si_4O_{11}Si_6^*$ depending on the local environment.

The second group is formed by "large" QM clusters. Some of these are built as natural extensions of small QM clusters to test the effect of the cluster size on the defect properties. These clusters satisfy the following two criteria: (i) *at least* all six Si* interface atoms of the small QM clusters and their oxygen neighbors are included in the QM cluster, and (ii) each of the new terminating Si* atoms should have only one oxygen atom from the QM cluster and three other neighbors from the rest of the nanocluster.

Another set of large QM clusters was built so that to accommodate medium range topological features identified as fingerprints for particular types of configurations of E' centers. For example, clusters used to describe puckered configurations similar to that shown in Fig. 1(a) fully include at least one ring that hosts a potential O_B atom. Thus built clusters have sizes from 48 ($Si_8O_{24}Si_{16}^*$) to 72 ($Si_{13}O_{37}Si_{22}^*$) QM atoms.

We note that the small QM clusters differ only by details of their geometrical structure while the number of atoms and the cluster topology is the same for all of them (with the exception of those at three-member rings). On the other hand, the large QM clusters differ by topology, due to disorder of the a-SiO_2 structure, and by the number of atoms.

The electronic structure of QM clusters was calculated using the unrestricted Hartree-Fock (UHF) method as implemented in GAUSSIAN 98 package.[50] Standard 6-31G basis sets were used on QM oxygen and silicon atoms. A specially optimized s-type basis function was centered on the interface Si* atoms.

3. Describing the interactions between classical ions

A QM cluster, together with the interface Si* atoms, is surrounded by two spherical regions of atoms treated classically. The inner region, i.e., the classical part of region I, is represented using the classical shell model[51] with the modified parameters of interatomic interactions taken from Ref. 43. These parameters were modified so that to account for polarization of oxygen ions through the shell model and to correctly reproduce the high-frequency dielectric constant of α quartz.

More specifically, we replaced the rigid atom model for oxygen ions by the shell model. The charges of the oxygen core and shell were chosen to be $+0.04e$ and $-1.24e$, respectively. The stiffness of the core-shell spring constant was optimized to reproduce the high-frequency dielectric constant of α quartz and found to be 11 eV/Å^2.

The interaction between ions in the external region of classical atoms, region II, is described using a rigid-ion model and the original BKS potentials.[43]

To test the consistency of the rigid and shell model classical potentials, we first compare the geometrical parameters and physical properties of α quartz calculated using these sets. It is convenient to define the size of the unit cell using the crystallographic notations a, b, and c for lengths of primitive vectors (with a being along the x axis, b being in the xy plane, and c is perpendicular to the xy plane). Then the values of a and b parameters calculated using the two sets of potentials differ by 0.07%, while c differs by 0.35%. To compare the internal structures, we calculated the difference in fractional coordinates of the atomic cores and found that the largest and average differences are 0.006 and 0.002, respectively. The bulk modulus changed by 4.4% from 40.1 GPa in the rigid model to 42.0 GPa in the shell model. Finally, the static dielectric constant changed by 0.4% for ϵ_{11}^{0} and ϵ_{22}^{0} and by 0.7% for ϵ_{33}^{0}.

To further test the performance of the two sets on potentials we fully relaxed the 648-atom supercell representing an a-SiO$_2$ structure using both sets and compared the geometrical parameters of the resultant structures. Both sets of potentials produce essentially the same geometrical parameters of the supercell with only 0.03% difference in the cell volume. The largest difference in the fractional coordinates of the corresponding atomic cores was 0.0016 which translates into 0.03 Å, while the average difference was 0.017 Å.

Overall, these tests indicate that the original rigid atom BKS potentials and their modified shell model version used in these calculations are compatible with sufficient accuracy.

In addition to the pairwise interactions described above, a set of classical three-body potentials of the form $(k/2)(\theta-\theta_0)^2$ was introduced at the interface between the QM cluster and the classical region to correct for the distortion of O-Si*-O and Si*-O-Si angles (θ) due to imperfect embedding. Since all O-Si-O and Si-O-Si angles in a-SiO$_2$ are different, the separate θ_0 parameters were defined to treat each such angle at the cluster border. The θ_0 parameters were taken as the corresponding angles in the original MD structure. The force constant of 4 eV/rad^2 was fitted so that to correct the corresponding angles in α quartz.

4. Perfect lattice test

To test the accuracy of the embedded cluster method and to compare with the results of previous studies we carried out the usual routine used in embedded cluster studies, which includes a so-called "perfect lattice test," i.e., full geometry optimization for the nondefective cluster. In the case of amorphous SiO$_2$ the reference "perfect" structure is the 648-atom periodic structure obtained in the MD calculations followed by the total energy minimization in the periodic model using the modified BKS potentials with shells on oxygen ions. The largest obtained changes in Si*-O bond lengths and Si*-O-Si angles with respect to the ideal structure were, 3%–5% and 5.5%, correspondingly. The obtained deviations of distances and angles in the rest of the system were several times smaller. The effective charges on ions obtained with natural population analysis (NPA) method[52] were in the range of $2.80\pm0.02e$ for silicon ions and $-1.35\pm0.01e$ for those oxygen ions which are not neighbors of interface atoms.

Importantly, the topology of the amorphous network in the QM region and at the interface remained the same as obtained from the original classical MD simulation. Moreover, the displacements of atoms as a result of the embedding procedure are relatively small. This allows us to establish a correlation between the quantum-mechanical and classical descriptions of the same lattice sites by comparing the Si-O distances at the center of each fully relaxed QM cluster with the corresponding distances in the classical calculations. We found that the Si-O distances in the QM calculations are systematically larger than those in the classical calculations by about 0.03 Å. In the following discussion we will correlate the defect properties with the geometrical parameters of the original amorphous structure. For clarity and consistency we will be using only a classical scale for the Si-O distances on the understanding that the QM distances are about 0.03 Å larger.

III. RESULTS OF CALCULATIONS

Building up a statistics of defect properties requires some guiding rule in choosing sites in amorphous structure. In this paper we assume that neutral oxygen vacancies can be formed at any oxygen site with the same probability, so their distribution follows the distribution of different sites in the original amorphous structure. E' centers are then formed as a result of ionization or hole trapping by pre-existing neutral oxygen vacancies. This approach allows us to find different structural types of positively charged vacancies.

A. Neutral oxygen vacancies

We selected 70 oxygen sites (out of total number of 432 for the 648 atom structure) to span the distributions of Si-O bond lengths, Si-O-Si angles and local topologies (ring structures). Two of these distributions are shown in Fig. 2. The characteristics of the chosen oxygen sites are shown by shaded areas in the same figure and demonstrate that most combinations of Si-O distances, Si-O-Si angles as well as ring sizes have been taken into account. In particular, about 30 out of the chosen sites correspond to different Si-O distances, another 30 cover the Si-O-Si angles distribution, and 10 cover all ring sizes.

The properties of these neutral oxygen vacancies were calculated using the "small" embedded QM clusters. All clusters were initially relaxed without the vacancy. Neutral vacancies were created by removing the central oxygen atom corner shared by the two tetrahedra comprising the cluster. The formation energies were calculated with respect to the total energy of the corresponding nondefective QM cluster and the oxygen atom in the triplet state.

The distribution obtained for the oxygen vacancy formation energies is shown in Fig. 3. It has a full width at the half-maximum of about 1.8 eV and peaks between 4.2 and 4.4 eV. The latter should be compared with the formation energy of 4.48 eV (Ref. 33) for the oxygen vacancy in α quartz calculated using a QM cluster of the same size. As discussed in earlier work,[33] the absolute value of the formation energy depends on the basis set and size of the QM cluster, but the shape and width of the distribution should not depend significantly on these parameters.

The large width of the formation energy distribution clearly indicates that some of the neutral vacancies in a-SiO$_2$ can differ significantly from that in α quartz. To characterize this difference we looked at several parameters, such as (i) charges on the two Si atoms near the vacancy; (ii) the displacements of the two Si atoms from their nondefective positions; and (iii) the distances of these two Si atoms from the centers of the respective neighboring oxygen planes.

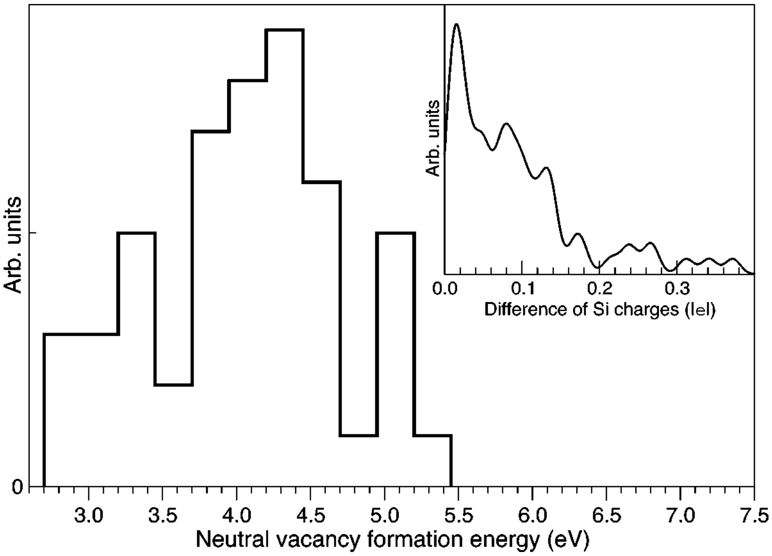

FIG. 3. Distribution of formation energies of neutral oxygen vacancies in a-SiO$_2$. The inset shows the distribution of differences in atomic charges of Si atoms near neutral oxygen vacancies. The statistics are taken over 70 sites.

In α quartz, the effective charges on the two Si atoms neighboring the neutral oxygen vacancy, calculated using the NPA method,[52] are 2.17e and 2.20e, i.e., are quite similar. The charges on Si atoms near the vacancy in a-SiO$_2$ vary from 1.89e to 2.29e, and the charge difference in corresponding pairs varies from 0.0e to 0.4e. The distribution of differences in atomic charges is shown in the inset of Fig. 3. Although the maximum of this distribution is close to the charge difference in α quartz, the majority of the vacancies have a more asymmetric charge distribution, indicating that in a-SiO$_2$ the two Si atoms are on average more dissimilar than in α quartz. This is confirmed by comparison of the displacements of the Si atoms neighboring the vacancy from their initial positions in the nondefective structure. In α quartz, these displacements are 0.5 Å and 0.3 Å, whereas in a-SiO$_2$ they vary from 0.2 Å to 0.5 Å. The two silicon atoms form pyramids with the remaining three oxygen ions of their corresponding tetrahedra. The distribution of distances from each Si atom to the center of the plane formed by the three neighboring oxygens shows similar behavior. In α quartz the corresponding distances are 0.573 Å and 0.565 Å, whereas in a-SiO$_2$ these distances vary from 0.45 Å to 0.72 Å, and their differences vary from 0.00 Å to 0.15 Å.

Further analysis of the medium and long range relaxation of the amorphous network induced by the formation of neutral vacancies demonstrates that, as in α quartz (see Ref. 33), this relaxation is very long ranged. However, the character of this relaxation can be even more complex. For example, in some cases the two Si atoms near the vacancy displace less than their neighboring oxygen atoms. This is accompanied by the large distortion of the Si-O-Si angles associated with the oxygen atoms. Since the tetrahedral O-Si-O angles do not change much (about 2°) the oxygen plane shifts with respect to the Si atom closer to the vacancy. Overall, the network relaxation shows compaction near the vacancy site.

B. Structural types of E' centers: Dimer and dangling bond

To build a preliminary picture of possible structural types of E' centers in a-SiO$_2$ we first carried out the calculations of positively charged vacancies using the "small" embedded QM cluster. The equilibrium structures of the E' centers were obtained by ionizing the neutral vacancies, described above, followed by full geometry optimization. Only 45 sites are considered in this further discussion as the E' centers at the other 25 sites induce network distortions too strong to be reproduced properly on the same level of accuracy using small clusters.

The distribution of the spin density between the two Si atoms near the vacancy (see Fig. 4) suggests that we have three types of positively charged vacancies in our amorphous structure. These can be called a dimer, a dangling bond type center, and an intermediate state.

To understand better the origins of these structural types of E' centers we attempt to link them with the local atomic

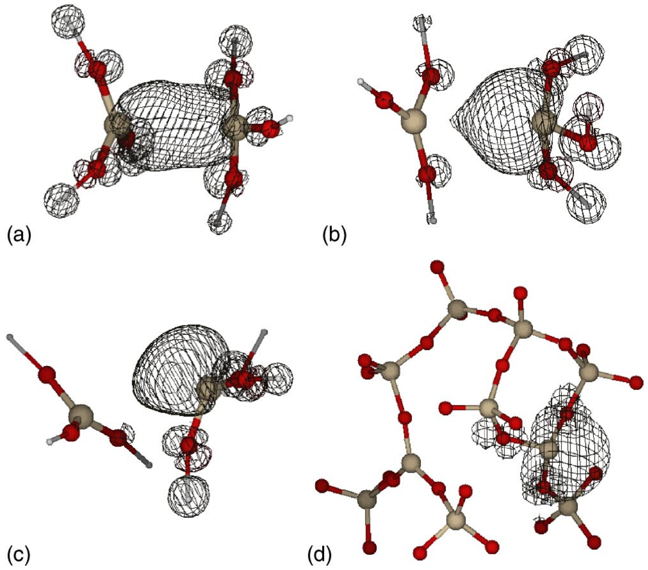

FIG. 4. (Color online) Spin density distributions in different types of E' centers: (a) dimer configuration, (b) intermediate configuration, (c) dangling bond (DB) configuration, (d) back-projected configuration. (a)–(c) were calculated using "small" QM clusters, (d) using a "large" cluster.

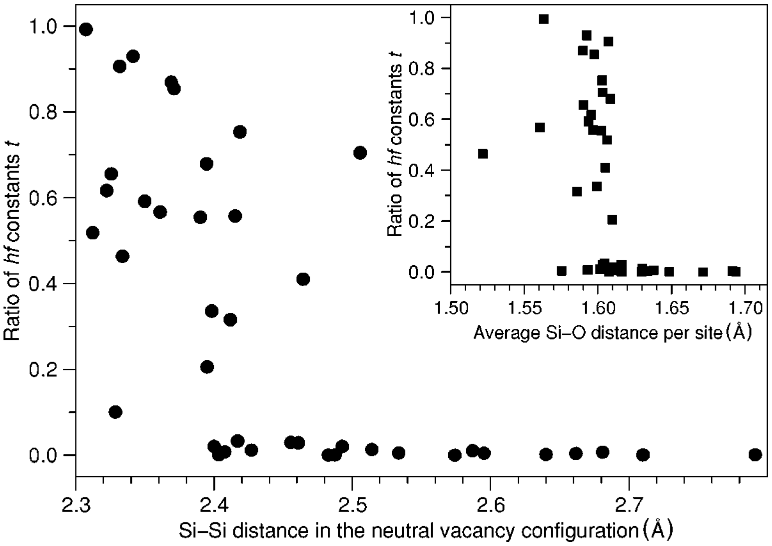

FIG. 5. Correlation of the ratio of the hyperfine constants on the neighboring Si atoms in the E' center configuration t with the Si-Si distance in the parent neutral vacancy. The inset shows the correlation between the same ratio of the Si hyperfine constants and the average Si-O distance at the corresponding oxygen site in the original amorphous structure.

structure of their precursors—neutral vacancies. For that purpose we introduce a parameter t—the ratio of hyperfine constants on the two Si ions a_{Si_1} and a_{Si_2} neighboring the vacancy, and correlate it with structural parameters of neutral vacancies. The parameter t is defined as $t=a_{\mathrm{Si}_1}/a_{\mathrm{Si}_2}$, where $a_{\mathrm{Si}_1}<a_{\mathrm{Si}_2}$. The dimer type configurations are characterized by similar hyperfine constants on both Si ions resulting in t being close to unity. In the dangling bond configuration, the spin density is almost completely localized on one Si ion and t is close to zero.

As one can clearly see in Fig. 4, the local structure of the parent neutral vacancy plays an important role in determining the type of the E' center formed. In particular, the difference in relative orientations of tetrahedral units surrounding the vacancy is clearly visible. To characterize this feature even further, in Fig. 5 we show the correlation between the Si-Si distance in the neutral vacancy configuration and the ratio t for the corresponding positively charged vacancies. One can see that, if the Si-Si distance in the precursor neutral vacancy is less than 2.4 Å, the ionized state shows the ratio t predominantly larger than 0.5 which corresponds to the dimer and some intermediate configurations. For the Si-Si distances between 2.4 Å and 2.5 Å one obtains the intermediate and dangling bond configurations. Longer distances always result in dangling bond configurations.

One can also distinguish three types of displacements of Si ions following the relaxation from a neutral vacancy into an ionized configuration. The formation of dimer type centers is characterized by relatively small displacements of atoms from their positions in the precursor neutral vacancy, rather similar to those in a dimer type E' center in α quartz (the Si displacements around 0.3 Å, maximum). In this case the two Si ions do not fall far apart so that Si-Si bond could still be preserved. The stronger relaxation from neutral vacancy (around 0.5 Å) is characteristic of intermediate type centers, and in most dangling bond centers the two Si ions find themselves much further apart with a large displacement (maximum of 1.0 Å) from the initial neutral vacancy configuration. This relaxation is determined by both the initial short and medium range structures and is accompanied by the reorientation of surrounding tetrahedra.

In simple terms, these results can be understood if one considers that each of the two Si ions surrounding the vacancy provides a potential well for the unpaired electron, so that the vacancy can be treated as a double-well potential problem. If the distance between the Si ions is small, the two wells merge into a single one. So long as the two Si ions are not much different, meaning that their combined potential well is not distorted towards one or the other, the dimer type center is formed. However, if the resulting potential well is asymmetric, the unpaired electron will tend to localize in the deeper well. The network relaxation will enhance this effect leading to the formation of a variety of structures including the dangling bond and intermediate configurations. It is important to realize that the probability of forming these configurations depends on the medium range order. If the distance between the two Si ions is large, even a small difference in the depth of their potential wells will be enough to produce a dangling bond type center. At small Si-Si distances, dangling bond type centers still can be created if the potential wells formed by the two Si ions are very different.

If neutral vacancies are formed with equal probability at any oxygen site in the original amorphous structure, what should be the relative concentrations of different types of configurations? In Ref. 30 we suggested that the average Si-O distance between the two silicon ions neighboring the same oxygen in the initial amorphous network, $D=(d_1+d_2)/2$ (see inset in Fig. 5) can serve as a useful parameter determining which type of positively charged oxygen vacancy could be formed at a particular oxygen site. This parameter takes into account that in the tetrahedral structure of silica the oxygen vacancy site is not directly on the Si-Si line. The plot of the ratio of hyperfine constants t as a function of the parameter D is presented in the inset of Fig. 5. It clearly demonstrates that for $D<1.62$ Å all defects are of the dimer or intermediate type, whereas for $D>1.62$ Å only dangling bond type defects are formed. One can therefore use D for predicting relative concentrations of different defect types.[30] However, as discussed in the appendix, the result depends on the calculation method: calculations using density functional theory and density functionals with small contribution of exact exchange tend to favor dimer configurations over dangling bonds.

To summarize, the calculations in small clusters predict three types of positively charged oxygen vacancy centers: the dimer, the dangling bond type center with unpuckered second Si ion, and several configurations intermediate between the two. The classical puckered E' center configurations could not be obtained in these calculations because the interaction of the puckering Si and the "back oxygen" O_B atoms could not be reliably described within small QM clusters. These configurations are considered below using larger QM clusters.

Our calculations predict long-range distortions of the amorphous structure, which extend to about 10 Å from the oxygen vacancy site. The character and range of these distortions is generally very similar to that reported earlier for α quartz.[34] However, unlike in quartz, they are characterized by broad variations and depends strongly on the short- and medium-range structure of the original network site where a defect was created.

C. Searching for other configurations

The E' center configurations found so far correspond to weakening or breaking of the Si-Si bond in the oxygen vacancy but do not include more complex puckered and back-projected configurations suggested in the literature. One of the reasons is that the network distortion induced by some of the defects cannot be properly treated in small QM clusters discussed above. Another reason could be that these configurations are quite rare or can be reached only after overcoming a potential barrier. As will be shown in the next section, to find these configurations more easily one can use some characteristic "fingerprints" deduced from previous analysis.

1. Puckered configuration of E' center

To find oxygen sites that are likely to host puckered positively charged oxygen vacancies we search for oxygen ions in the original a-SiO_2 structure that can serve as back oxygens, O_B, for stabilizing puckered Si ions after relaxation of charged vacancies.

For this purpose we first analyze the structure of the puckered configuration of the E'_1 center in α quartz. The structure of this crystal is characterized by so-called short and long Si-O bonds. The predicted most stable configuration of E'_1 center is associated with puckering of Si_L through the plane of its oxygen neighbors and bonding with O_B, which is its fifth neighbor in the undistorted lattice [see Fig. 1(a)]. Such puckering is not possible for the Si_S because there is no oxygen ion among its neighbors, which would stabilize Si_S in the PC. Thus, the medium range environment of a Si ion near an oxygen vacancy determines whether it will or will not be stable in the PC.

Detailed analysis of the local atomic structure of the Si_L and O_B sites in quartz suggests that the Si_L-O_B bonding in the PC of the E'_1 center is due to their favorable relative geometrical orientation. In particular, the triangle formed by O_B and its two Si neighbors (Si_{B1}-O_B-Si_{B2}) is oriented by its O_B vertex approximately towards the Si_L ion [Fig. 1(a)]. Taking into account the flexibility of the Si-O-Si angles, we expect strong relaxation of Si_{B1}-O_B-Si_{B2} towards Si_L to form the Si_L-O_B bond and thus stabilize it in the PC. On the contrary, none of the medium range oxygen neighbors of the Si_S are pointing to it in a similar way. We exploit this observation to introduce a numerical criterion for the likelihood of the E'_γ center formation at a given site in a-SiO_2. Again, we assume that all sites in a-SiO_2 are amenable to formation of E'_γ centers. Then we need to find which Si ions can be stabilized by their medium range oxygen neighbors in the same way as by O_B in α quartz.

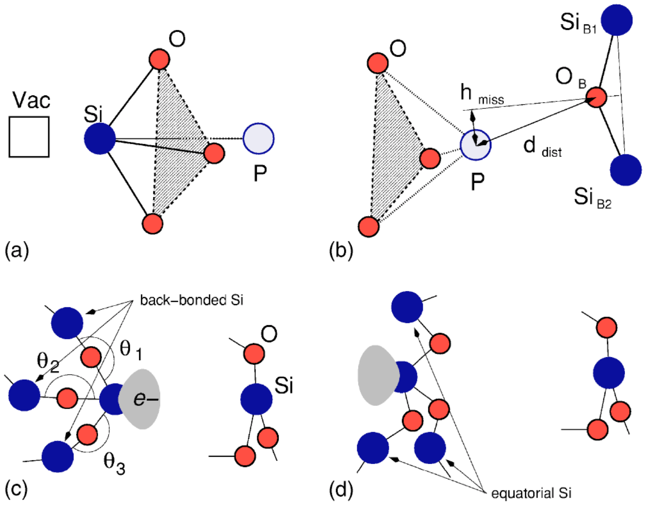

FIG. 6. (Color online) (a), (b) A criterion used to search for O_B in a-SiO_2 structures. (a) Si ion in the puckered configuration will be close to site P obtained by the reflection of Si in the plane of its nearest oxygen neighbors. (b) illustrates two numerical parameters for O_B search, O_B-P distance (d_{dist}) and "near miss" distance (h_{miss}). (c) and (d) Criterion used to search for sites in a-SiO_2 structures that can form a back-projected configurations. (c) Si_1 will be a candidate for back projection if all Si_1-O-Si angles θ_1, θ_2, θ_3 in the nondefective lattice will be around 180°. (d) The back-projected configuration after the formation of E' center.

To search for O_B in a-SiO_2 we first postulate that in the case of a stable E'_γ puckered Si ion will occupy a site P defined by reflection of the Si ion in the undistorted lattice in the plane of its three nearest oxygen neighbors as shown in Figs. 6(a) and 6(b). Then we search for all oxygen neighbors (nearest neighbors excluded), which (i) are close to point P, and (ii) belong to a Si-O-Si unit pointing towards point P.

Parameters d_{dist} and h_{miss} define a "fingerprint" for the E'_γ center. The numerical values for d_{dist} and h_{miss} for each site are extracted from the calculation of the E'_1 center.[34] If an oxygen ion is found that $d_{dist} < 2.6$ Å and $h_{miss} < 0.6$ Å, which is the case for Si_L in α quartz, then the corresponding Si ion is expected to be stabilized in the puckered configuration. If, however, an oxygen ion is found that $d_{dist} > 4.2$ Å and $h_{miss} > 0.8$ Å, which is true for Si_S in α quartz, then the corresponding Si will not pucker. The intermediate cases need to be considered separately so that the values of d_{dist} and h_{miss} critical for the E'_γ center formation could be established.

We used these criteria to identify all the potential sites capable of accommodating the puckered E'_γ configuration in the nondefective amorphous structure and found that their

TABLE II. Hyperfine constants (mT) for E' centers formed at different sites. Sin $(n=1,2)$ and Si_{ni} $(i=1,2,3)$ are the nearest and the second nearest neighbors of the oxygen vacancy, respectively.

				Si_{1i} *shf*				Si_{2i} *shf*		
Type of E' defect	QM cluster	Figures	Si_1 *hf*	Si_{11}	Si_{12}	Si_{13}	Si_2 *hf*	Si_{21}	Si_{22}	Si_{23}
Dimerlike	$Si_{13}O_{37}Si*_{22}$	7(a)	10.9	0.08	0.17	0.04	12.1	0.05	0.35	0.35
E'_{DB}, unpuckered	$Si_{10}O_{29}Si*_{18}$	7(c)	44.3	1.33	0.50	0.07	0.0	0.03	0.00	0.00
E'_{DB}, puckered with O_B	$Si_{13}O_{37}Si*_{22}$	7(d)	43.0	1.13	0.80	0.20	0.0	0.00	0.00	0.00
E'_{DB}, back-projected	$Si_8O_{24}Si*_{16}$	7(e)	43.1	0.26	0.23	0.29	0.0	0.00	0.00	0.00
E'_{DB}, back-projected with O_B	$Si_{13}O_{37}Si*_{22}$	7(g)	48.9	0.45	0.02	0.25	0.0	0.00	0.00	0.00
E'_{δ}, Experimental (Ref. 15)			10.0							
E'_{γ}, Experimental (Ref. 53)			41.9	1.3	0.3					
E'_{γ}, Experimental (Ref. 54)			41.9	0.8	0.3					

number does not exceed 10% of all oxygen sites.

Then the embedded cluster calculations of positively charged vacancies were performed at three representative sites using QM clusters including up to 72 ions. Calculations were made first for the nondefective network, then for the neutral oxygen vacancy, and finally for the positively charged vacancy. We found both the unpuckered and puckered configurations for the same defect, but the puckered configuration was the most stable. It is interesting to note that whether the hole-bearing silicon ion is puckered or unpuckered does not significantly affect the hyperfine parameters of the E' center. The calculated isotropic hf constants for one of the puckered configurations given in Table II are representative of all configurations obtained.

Our analysis also demonstrates that the interaction of the puckering Si ion and the O_B is predominantly electrostatic. The latter observation allows us to make further qualitative analysis of puckered configurations using a fully classical approach. Using the shell model potentials and effective ionic charges on the Si ions near the vacancy we have calculated the relative energies of the puckered and unpuckered configurations for 16 vacancy sites.

We found a wide distribution where in some cases the back oxygen is located in a much more favorable position than that in α quartz and therefore is forming a much stronger bond with the puckering silicon ion. There are also opposite cases where the puckered configuration is less favored than the unpuckered dangling bond configuration.

2. *Back-projected configuration of E' center*

Another E' center type, not previously predicted theoretically, is the so-called back-projected configuration suggested by Griscom and Cook.[20] They pointed out that analysis of superhyperfine constants of E' centers may provide some insight into the medium range glass structure around them and suggested the geometric criteria for formation of the back-projected configuration based on dihedral and Si-O-Si angles. In simple terms, these criteria imply that, if all three Si-O-Si angles [θ_1, θ_2, θ_3 in Fig. 6(c)] with the so-called back bonded silicon ions in the nondefective lattice or in the neutral vacancy configuration are close to 180°, then the E' center formed at this site is likely to become back-projected after relaxation, as shown in Fig. 6(d). In other words, it will not have any back bonds at all. Based on this analysis they estimated that 35%–80% of all E' centers in their sample have this property. They are characterized by hyperfine constants of about 41.9 mT and superhyperfine constants of 0.3 mT. In this paper we are interested only in stability of such configurations and do not address the possible mechanism of their formation.

We have analyzed the 648-atom amorphous structure and found only three Si sites that approximately satisfy these criteria with Si-O-Si angles in the range of 170°–180°. We considered these sites using embedded QM clusters $Si_{10}O_{29}Si^*_{18}$, $Si_{13}O_{37}Si^*_{22}$, and $Si_{18}O_{24}Si^*_{16}$. The first QM cluster contains four- and six-member rings; the second contains three-, four-, and six-member rings, and the third contains only a three-member ring, correspondingly. The neutral, positively charged and back-projected configurations of the oxygen vacancy were calculated in these clusters. It turns out that in all cases the transformation from the initial dangling bond or dimer configuration into a back-projected one required overcoming a potential barrier of about 1.5 eV. The back-projected configurations found in our calculations are about 0.5 eV less stable than the normal, forward-projected, ones. However, calculated barriers for the transitions from the back-projected to the normal configurations are close to 1.0 eV. This suggests that, once formed, these configurations could remain stable up to high temperatures.

To estimate the percentage of sites that can give rise to a metastable back-projected configuration, we have carried out the following analysis. First, we noted that a Si atom in the back-projected configuration occupies a site close to the point P introduced above [see also a schematic in Fig. 6(b)]. To estimate the amount of free space available for a Si atom in the back-projected configurations we have calculated the smallest distance from the point P to the nearest host lattice atom D_{PA} (excluding the oxygen neighbors of the Si atom in question) and built the distribution of such distances for the

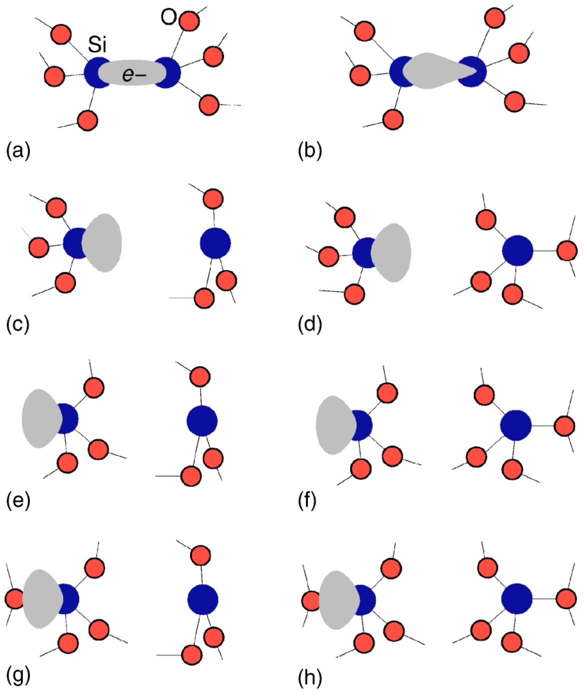

FIG. 7. (Color online) Possible types of E' centers suggested on the basis of medium range order in a-SiO$_2$. (a) Dimer; (b) intermediate (distorted dimer); (c) unpuckered dangling bond (DB) type: the unpaired electron is fully localized on a single Si atom, while the other Si atom moves to the plane of the neighboring oxygens; (d) puckered, similar to (c) but the second Si atom is tetrahedrally coordinated due to the presence of back oxygen; (e) back-projected DB, similar to (c) but the spin density due to the unpaired electron is projected away from the vacancy; (f) back-projected puckered DB; (g) back-projected back-puckered DB; (h) back-projected doubly puckered DB.

whole 648-atom a-SiO$_2$ structure. This distributions spans the region from 1.8 Å to about 3.7 Å with the maximum at approximately 2.8 Å. The smallest D_{PA} distance calculated for a stable back-projected configuration was found at 2.60 Å. This value defines a minimal amount of free space that is sufficient to stabilize a Si atom in the back-projected configuration. We found that about 67% of the lattice sites have the D_{PA} distance larger than 2.60 Å. We note that there seems to be a correlation between the free volume near point P and the stability of the back-projected configurations. For example, for the sites with D_{PA} equal to 2.60 Å and 2.75 Å the energies of the back-projected configurations are 0.95 eV and 0.55 eV higher than those for the corresponding forward-projected ones.

3. Stability of "intermediate" configurations

The results presented above clearly demonstrate that the potential energy landscape of positively charged oxygen vacancies is complex and may involve several minima. Therefore, one could expect that configurations intermediate between well-defined dimers and dangling bond centers [see Figs. 7(b), 7(a), and 7(c), respectively] may in fact be metastable and transform into more stable configurations of either type. To investigate this point we explored the adiabatic potential energy surface for four intermediate configurations. These configurations, initially obtained in small clusters, were now relaxed using large clusters which differ by the number and length of rings fully included in the QM cluster. For example, the 72-atoms cluster Si$_{13}$O$_{37}$Si$^*_{22}$ included three-, four-, and six-member rings and the Si$_{11}$O$_{31}$Si$^*_{18}$ cluster contained one four- and two five-member rings. Again calculations were repeated first for the nondefective network, then for the neutral oxygen vacancy, and finally for the positively charged vacancy. We found that the configurations with the value of the parameter t greater than about 0.45 (see Fig. 5) become closer to what one can call a dimer when relaxed using a large QM cluster. As a result the parameter t increases to 0.75 or more and the values of hyperfine constants on two Si ions near the vacancy site are ranging between 7 mT and 13 mT. Some configurations with t smaller than about 0.45, when calculated using a large cluster, become closer to dangling bond type E' centers [Fig. 7(c)] with t closer to zero. These calculations indicate that the definition of dimer should include some of the distorted configurations. However, we should conclude that small cluster calculations may not be sufficient for accurate description of the electron density distribution within E' centers formed at certain sites and for prediction of relative concentrations of different configurations.

4. Hyperfine parameters

To calculate the hyperfine parameters of E' center configurations discussed above we used quantum clusters listed in Table II. Several configurations were chosen from the distribution shown in Fig. 5. We traced back the initial oxygen sites in the amorphous network. Then a quantum cluster was constructed around each of these sites and calculations were repeated first for the nondefective network, then for the neutral oxygen vacancy, and finally for the positively charged vacancy. The obtained geometrical parameters of neutral and charged vacancies are close to those obtained using small clusters. The electronic structure of charged vacancies corresponds to the defect types they were initially chosen from. However, calculating in larger clusters does not confine the defect wave function and therefore gives a more reliable spin density distribution and hyperfine interaction with the nuclei of surrounding ions. In particular, the hf interaction of an unpaired electron of the dangling bond E' center calculated in small clusters is around 55 mT, and becomes 43 mT in large clusters. The hyperfine and superhyperfine constants obtained for the typical defect configurations are presented in Table II.

The calculated hyperfine constants on the two silicon ions of the fully symmetrical dimer configuration ($t=1$) are about 10 mT. Most of the spin density in this case is localized in the middle between the two Si ions as shown in Fig. 4(a) and schematically in Fig. 7(a). The hyperfine interaction with the nuclei of other Si ions is quite small, suggesting that the defect is strongly localized.

The hyperfine constants for the dangling bond configurations presented in Table II are for the defects with t very close to zero, i.e., for the spin density localized predominantly on one silicon ion. The hyperfine constants for these configurations form a distribution of values. In particular, the largest and the smallest hyperfine interactions with a Si ion which can be sensibly attributed to the dangling bond configurations are 46 mT and 38 mT, respectively. This is in agreement with the large signal broadening for E'_γ defects observed in EPR experiments.[15]

The hyperfine parameters calculated for one of the back-projected configurations are also presented in Table II. According to Griscom and Cook[20] and to the more recent review by Griscom,[12] E'_γ centers in this configuration are characterized by the so-called "weak" hyperfine constants of 0.3 mT, which are much smaller than those for the puckered configuration [see also Figs. 4(d) and 7(e)]. As one can see in Table II, our results are in a very good agreement with this prediction. We found that in several cases the hyperfine splitting for the "equatorial" Si atoms in a back-projected E' center are indeed just under 0.3 mT (see Table II). However, this value may vary in the range of 0.0–0.5 mT from site to site. In other words, similar to previous cases, there is a distribution of geometrical parameters of these configurations and in the corresponding values of hyperfine constants.

IV. DISCUSSION

A consistent picture emerges from our work for the possible configurations of neutral and positively charged oxygen vacancies in amorphous silica. Neutral vacancies are characterized by a wide distribution of formation energies and structural parameters. Positively charged vacancies form two major structural types: dimer and dangling bond centers. We predict that the most dangling bond centers are unpuckered [see Fig. 7(c)] and demonstrate that most configurations of the dangling bond centers have similar hyperfine EPR parameters. Our results confirm the possibility of existence of the back-projected E'_γ center configuration and suggest that such centers can be stable in a larger number of sites than has been proposed from the experiment[20] [see Figs. 7(e)–7(h)]. We also suggest that the puckered configuration is not the dominant configuration of E'_γ center in amorphous silica.

Our approach differs from those used in similar previous studies in several respects. Many molecular cluster calculations (see, for example, Refs. 17, 22, and 48) are not based on any particular a-SiO$_2$ model and so can capture only those defect properties which are determined by the most stable *local* properties of the material. Our calculations explore a well-established model of an amorphous structure and allow us to treat consistently the local, medium range, and long range environment of each defect site. In addition we can build a statistical distribution of defect properties and relate these properties to the structure of the amorphous network. Besides, the embedded cluster model allows one to properly account for variations of the electrostatic potential in the amorphous network and for its polarization by the charged defect.

Recent studies[23,29] have used a similar approach to building a distribution of defect properties. However, they employed a periodic DFT computational technique and a much smaller 72 atom periodic cell. Our calculations allow us to take into account the defect-induced relaxation of a much larger region. They employ the Hartree-Fock method in the local basis set. Although some of the results obtained in our work and in Refs. 23 and 29 are qualitatively similar, there are important differences discussed below, partly from region size, and partly from differences between HF and DFT.

The dimer type configuration has been predicted as one of the two configurations of the positively charged vacancy in quartz and in several calculations modeling amorphous silica.[17,23,29,55,56] This configuration has been proposed as a structural model of the E'_δ center[17] on the basis of a good agreement between the calculated and experimental hf constants. We note that in our calculations the dimer configuration occurs naturally as a result of ionization of some neutral vacancies rather than by construction of a cluster.[17,55] We also predict the hf constants on the two Si ions of the dimer close to those measured experimentally for the E'_δ center.[16,20] The main reason for these relatively small values of the hf interaction, which are incidentally approximately four times smaller than the hf interaction in the dangling bond configuration (see Table II), can be also explained by our calculations. As one can see in Fig. 4, the spin density in the dimer configuration is localized to a large extent between the two Si ions reducing the *s* orbital contribution on the Si nuclei. We did not consider more complex structural models proposed for the E'_δ center[15,16,18] and cannot comment on their feasibility. One cannot exclude, however, that simple dimers may coexist with these more complex defects in some samples. This question requires further investigation as well as elucidation of optical properties of these centers.

We note that our results predict that dimers are the minority species with respect to other positively charged oxygen vacancies rather than the majority species predicted in Refs. 23 and 29. As discussed in the appendix, this discrepancy between the two studies results from the different methods used: plane wave DFT tends to delocalize weakly bound electronic states, which led to the disproportionally large number of dimers obtained in Ref. 23 and 29. On the other hand, the Hartree-Fock method used in this work tends to favor localized solutions. The very fact that we obtained several dimer configurations in strongly disordered structure using this method testifies in favor of their existence. However, we should note that most of these configurations are distorted and for some types of local environment of these vacancies we find that there exists the second more stable dangling bond type configuration.

It is interesting to note that the unpuckered DB configuration basically corresponds to that suggested by Yip and Fowler[57] as model of E'_1 center on the basis of small cluster calculations some 30 years ago. But it has never actually been *predicted* in theoretical calculations of amorphous structures. Moreover, some works[21] concluded that the ionization of a neutral vacancy would always produce a dimer configuration (with the exception of vacancies formed on the edge of edge-sharing tetrahedra). The typical hf and shf constants for the unpuckered E' center configuration are given in Table II. The hf constants of the DB-type defects are similar to those assigned to the E'_γ center in a-SiO$_2$ in experimental[20,28] and other theoretical[11,22,25,56] studies. However, unlike in the case of the E'_γ center, this configuration does not require any back oxygen (O$_B$). Our calculations suggest that this could be the most abundant type of E' center obtained by ionizing pre-existing neutral vacancies in amorphous silica. Other types, such as the puckered and back-projected configurations require more specific conditions for their stabilization. We note, however, that our calculations suggest that the conditions for existence of stable back-projected E' centers are much less strict than originally suggested in Ref. 20. In fact, only a sufficiently large void space is required to stabilize E' centers in the back-projected configuration.

The hf constants given in Table II belong to different kinds of DB-type E' centers, distinguished by their shf constants. The hf constants of these centers are similar and fall within the full width at half-maxima (FWHM) of E'_γ center in a-SiO$_2$. The shf constants for the unpuckered E' centers and classically puckered E' centers are similar as both have a weak shf constant of about 1.1 mT. For back-projected E' centers, the Si atom possessing the unpaired electron points away from the vacancy and there is no weak shf interaction, but only very weak shf interaction, as observed experimentally.[19,20]

Our calculations demonstrate the strong long range lattice relaxation induced by most of the oxygen vacancies. This effect cannot be fully accounted for using molecular clusters and periodic calculations. This might be one of the reasons why earlier theoretical calculations could not predict, e.g., the unpuckered DB-type defect. Other configurations may also exist although we did not find them. Extending the behavior of the Si atoms we predicted that there could be, for example, double puckering when both the Si atoms have back oxygen atoms (O_B) [see Fig. 7(h)], and even more complex configurations.

Configurations discussed above were obtained by single ionization of a precursor neutral vacancy. In reality, though, precursor sites for defect creation depend on the mechanism of defect formation. On the one hand, there is no clear reason to believe that neutral vacancies are formed with the same probability at any site in amorphous structure, as assumed in this paper. On the other hand, in irradiated samples E' centers are formed due to exciton decomposition into a pair of Frenkel defects.[58] In this case, the structure and the spatial distribution of defects depend on where stable defects can be formed in a particular amorphous structure and on their diffusion properties. In most cases silica samples are irradiated by large doses of ionizing radiation or by powerful laser pulses. In this case, multiple secondary processes involving sequential electron trapping and ionization of the same defect can be important. These processes can tip the balance of different configurations increasing the concentration of, e.g., back-projected or even more complex configurations shown in Fig. 7.

Our results, like those of previous workers, clearly highlight issues which should be addressed in further studies. The key issue remains an accurate prediction of relative concentrations of different defect types. It is hampered by several factors. First, it is based on an assumed mechanism of formation of positively charged vacancies via hole trapping by neutral vacancies. One should take into account the distribution of neutral vacancy formation energies and radiation mechanisms via exciton decomposition into defect pairs, which both may lead to inhomogeneous (and different) distributions of defects. Second, the defect types (dimer vs dangling bond) formed in particular network sites are sensitive to the quantum-mechanical method used in calculations. This does not allow one to apply reliably the structural criteria relating defect types to the structural properties of individual sites in the amorphous network ("fingerprints") in order to predict possible defect concentrations.

ACKNOWLEDGMENTS

The authors would like to thank S. Agnello, M. Cannas, A. H. Edwards, W. B. Fowler, D. L. Griscom, V. Mashkov, L. Skuja, V. B. Sulimov, K. Tanimura, A. N. Trukhin, and K. Mallik for many useful discussions. We acknowledge the HPCx parallel computer facility for calculations. The work is supported by EPSRC, Japan Science and Technology Corporation, US Airforce through EOARD, and by the Grant-in-Aid for Creative Scientific Research (No. 16GS0205) from the Japanese Ministry of Education, Culture, Sports, Science and Technology. The computer time on the HPCx facility was awarded to the Materials Chemistry consortium under EPSRC Grant No. GR/S13422/01 Materials Chemistry using Tera-scale Computing.

APPENDIX: DESCRIPTION OF THE E' CENTERS USING DIFFERENT QM METHODS

We have stated previously that the relative concentration of different configurations of E' centers can depend on the method that is used for the electronic structure calculations. This appendix aims to characterize such a dependence in more detail.

We use the embedded cluster approach, as described above in Sec. II, to compare the electronic structures and the local atomic configurations of positively charged oxygen vacancies (E' centers) calculated using two different *ab initio* schemes: the unrestricted Hartree-Fock (UHF) and a hybrid density functional B3LYP. The latter combines Becke's three parameters hybrid exchange functional[59] containing the exact exchange contribution and the correlation functional by Lee, Yang, and Parr.[60] Several (17) oxygen vacancy sites in a-SiO$_2$ were randomly selected for these calculations. Topologically identical "small" QM clusters Si_3^*-O_3-Si-Vac-Si-O_3-Si_3^* were used so that to allow one to compare the results obtained for different sites. In all of the calculations we fully relax region I and then analyze the electronic structure and atomic configuration of each E' center.

Then the E' types can be classified in terms of the ratio of the two hyperfine constants t defined earlier. The results of the analysis are summarized in Fig. 8, where we correlate the hyperfine constants on Si$_1$ and Si$_2$ with the structure of the E' center. The thick solid line in this figure corresponds to $t=1.0$ and, therefore, the "ideal" dimer configurations should be positioned along this line. The abcissa axis corresponds to $t=0.0$, i.e., to the "ideal" dangling bond configurations. The open triangles and the shaded squares show the configurations calculated using the UHF and B3LYP, respectively.

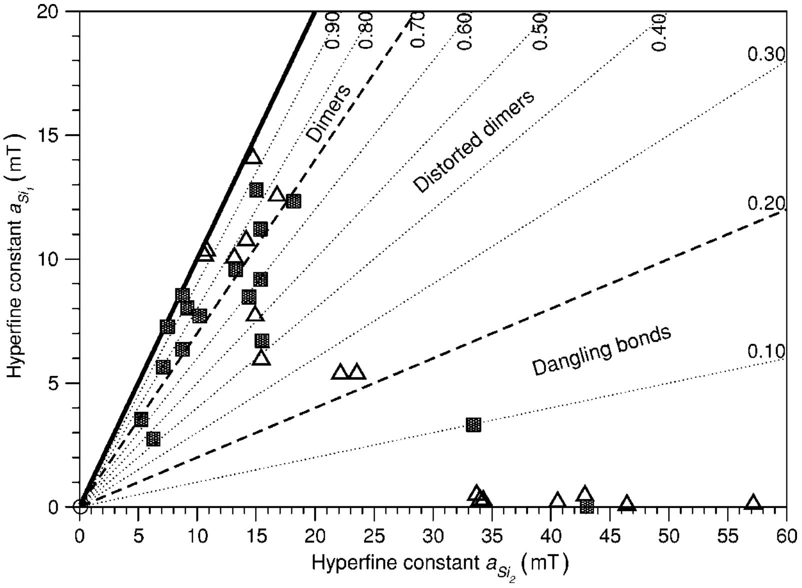

FIG. 8. Hyperfine constants and character of E' centers calculated using UHF (open triangles) and B3LYP (shaded squares). Dotted lines show the ratio $t = a_{\mathrm{Si}}/a_{\mathrm{Si}_2}$. The thick solid line corresponds to ideal dimer type configurations. The two dashed lines show an approximate division of all centers in the three types of dimer, dangling bonds and intermediate configurations (distorted dimers).

One can see that the ideal dimers are relatively scarce: the UHF produces three such configurations and the B3LYP produces two. At the same time, we found that UHF gives seven dangling bond type centers, while only one such configuration was found with B3LYP. All other configurations are scattered across the field and correspond to somewhat distorted dimers. To characterize this distribution further we can introduce loose boundaries between the dimers and distorted dimers at $t = 0.7$ and between the distorted dimers and dangling bonds at $t = 0.2$. Then the UHF results in six dimers, four distorted dimers, and seven dangling bonds, while B3LYP gives nine dimers, six distorted dimers, and only two dangling bonds for *the same* selection of sites.

The qualitative difference in the number of dimer configurations obtained using the UHF and hybrid density functional does not depend on the cluster size. It is consistent with the already well-documented tendency of DFT to favor delocalized density distributions. On the other hand, UHF favors localized solutions due to lack of correlation. These issues are related to the self-interaction error in DFT which has been analyzed in detail, for example, in Ref. 61. Some of the implications of this problem with respect to self-trapping and polaron formation problems have recently been discussed in Refs. 35 and 62.

---

*Corresponding author. Email address: s.mukhopadhyay@ucl.ac.uk
†Corresponding author. Email address: a.shluger@ucl.ac.uk

[1] *Defects in SiO_2 and Related Dielectrics: Science and Technology*, edited by G. Pacchioni, L. Skuja, and D. L. Griscom, NATO Science Series, Series II: Mathematical and Physical Chemistry (Kluwer Academic, Dordrecht, 2000).

[2] *Structure and Imperfections in Amorphous and Crystalline Silicon Dioxide*, edited by R. A. B. Devine, J.-P. Duraud, and E. Dooryhée, (Wiley, New York, 2000).

[3] A. C. Wright, *Defects in SiO_2 and Related Dielectrics: Science and Technology* (Kluwer Academic, Dordrecht, 2000), Chap. Defect-free vitreous networks: The idealised structure of SiO_2 and related glasses, pp. 1–35, NATO Science Series, Series II: Mathematical and Physical Chemistry.

[4] M. A. Szymanski, A. L. Shluger, and A. M. Stoneham, Phys. Rev. B **63**, 224207 (2001).

[5] A. Bongiorno and A. Pasquarello, Phys. Rev. Lett. **88**, 125901 (2002).

[6] R. A. Weeks and C. M. Nelson, J. Am. Ceram. Soc. **43**, 399 (1960).

[7] R. H. Silsbee, J. Appl. Phys. **32**, 1456 (1961).

[8] M. G. Jani, R. B. Bossoli, and L. E. Halliburton, Phys. Rev. B **27**, 2285 (1983).

[9] J. K. Rudra and W. B. Fowler, Phys. Rev. B **35**, 8223 (1987).

[10] D. C. Allan and M. P. Teter, J. Am. Ceram. Soc. **73**, 3247 (1990).

[11] M. Boero, A. Pasquarello, J. Sarnthein, and R. Car, Phys. Rev. Lett. **78**, 887 (1997).

[12] D. L. Griscom, *Defects in SiO_2 and Related Dielectrics: Science and Technology* (Kluwer Academic, Dordrecht, 2000), Chap. The natures of point defects in amorphois silicon dioxide, pp. 117–160, NATO Science Series, Series II: Mathematical and Physical Chemistry.

[13] P. M. Lenahan and J. J. F. Conley, J. Vac. Sci. Technol. B **16**, 2134 (1998).

[14] A. Stesmans, B. Nouwen, and V. V. Afanas'ev, Phys. Rev. B **66**, 045307 (2002).

[15] D. L. Griscom and E. J. Friebele, Phys. Rev. B **34**, 7524 (1986).

[16] L. Zhang and R. G. Leisure, J. Appl. Phys. **80**, 3744 (1996).

[17] J. R. Chavez, S. P. Karna, K. Vanheusden, C. P. Brothers, R. D. Pugh, B. K. Singaraju, W. L. Warren, and R. A. B. Devine, IEEE

Trans. Nucl. Sci. **44**, 1799 (1997).

[18] R. Tohmon, Y. Shimogaichi, Y. Tsuta, S. Munekuni, Y. Ohki, Y. Hama, and K. Nagasawa, Phys. Rev. B **41**, 7258 (1990).

[19] S. Agnello, R. Boscaino, G. Buscarino, M. Cannas, and F. M. Gelardi, Phys. Rev. B **66**, 113201 (2002).

[20] D. L. Griscom and M. Cook, J. Non-Cryst. Solids **182**, 119 (1995).

[21] T. Uchino, M. Takahashi, and T. Yoko, Phys. Rev. Lett. **86**, 5522 (2001).

[22] T. Uchino, M. Takahashi, and T. Yoko, Phys. Rev. B **62**, 2983 (2000).

[23] Z.-Y. Lu, C. J. Nicklaw, D. M. Fleetwood, R. D. Schrimpf, and S. T. Pantelides, Phys. Rev. Lett. **89**, 285505 (2002).

[24] D. Donadio, M. Bernasconi, and M. Boero, Phys. Rev. Lett. **87**, 195504 (2001).

[25] A. Stirling and A. Pasquarello, Phys. Rev. B **66**, 245201 (2002).

[26] H. Hosono, H. Kawazoe, and N. Matsunami, Phys. Rev. Lett. **80**, 317 (1998).

[27] H. Hosono and N. Matsunami, Nucl. Instrum. Methods Phys. Res. B **141**, 566 (1998).

[28] M. Guzzi, M. Martini, A. Palear, F. Pio, A. Vedda, and C. B. Azzoni, J. Phys.: Condens. Matter **4**, 8635 (1992).

[29] C. J. Nicklaw, Z.-Y. Lu, D. M. Fleetwood, R. D. Schrimpf, and S. T. Pantelides, IEEE Trans. Nucl. Sci. **49**, 2667 (2002).

[30] S. Mukhopadhyay, P. V. Sushko, A. H. Edwards, and A. L. Shluger, J. Non-Cryst. Solids (to be published).

[31] S. Agnello, R. Boscaino, F. M. Gelardi, and B. Boizot, J. Appl. Phys. **89**, 6002 (2001).

[32] F. J. Feigl, W. B. Fowler, and K. L. Yip, Solid State Commun. **14**, 225 (1974).

[33] V. B. Sulimov, P. V. Sushko, A. H. Edwards, A. L. Shluger, and A. M. Stoneham, Phys. Rev. B **66**, 024108 (2002).

[34] A. S. Mysovsky, P. V. Sushko, S. Mukhopadhyay, A. H. Edwards, and A. L. Shluger, Phys. Rev. B **69**, 085202 (2004).

[35] G. Pacchioni, F. Frigoli, D. Ricci, and J. A. Weil, Phys. Rev. B **63**, 054102 (2001).

[36] P. V. Sushko, A. L. Shluger, and C. R. A. Catlow, Surf. Sci. **450**, 153 (2000).

[37] W. P. Hess, A. G. Joly, D. P. Gerrity, K. M. Beck, P. V. Sushko, and A. L. Shluger, J. Chem. Phys. **115**, 9463 (2001).

[38] J. S. Braithwaite, P. V. Sushko, K. Wright, and C. R. A. Catlow, J. Chem. Phys. **116**, 2628 (2002).

[39] P. V. Sushko, J. L. Gavartin, and A. L. Shluger, J. Phys. Chem. B **106**, 2269 (2002).

[40] P. V. Sushko, A. L. Shluger, K. Hayashi, M. Hirano, and H. Hosono, Phys. Rev. Lett. **91**, 126401 (2003).

[41] K. Vollmayr, W. Kob, and K. Binder, Phys. Rev. B **54**, 15808 (1996).

[42] W. Smith and T. R. Forester, J. Mol. Graphics **14**, 136 (1996).

[43] B. W. H. van Beest, G. J. Kramer, and R. A. van Santen, Phys. Rev. Lett. **64**, 1955 (1990).

[44] A. Navrotsky, Diffus. Defect Data **53/54**, 61 (1987).

[45] N. F. Mott and M. J. Littleton, Trans. Faraday Soc. **34**, 485 (1938).

[46] A. L. Shluger, E. A. Kotomin, and L. N. Kantorovich, J. Phys. C **19**, 4183 (1986).

[47] A. L. Shluger and J. D. Gale, Phys. Rev. B **54**, 962 (1996).

[48] G. Pacchioni, G. Ieranò, and A. M. Márquez, Phys. Rev. Lett. **81**, 377 (1998).

[49] D. Erbetta, D. Ricci, and G. Pacchioni, J. Chem. Phys. **113**, 10744 (2000).

[50] M. J. Frisch *et al.*, GAUSSIAN 98 (Revision A.7), Gaussian Inc., Pittsburgh, PA, 1998.

[51] B. G. Dick and A. W. Overhauser, Phys. Rev. **112**, 90 (1958).

[52] A. E. Reed, R. B. Weinstock, and F. Weinhold, J. Chem. Phys. **83**, 735 (1985).

[53] D. L. Griscom, Phys. Rev. B **20**, 1823 (1979).

[54] T. E. Tsai and D. L. Griscom, J. Non-Cryst. Solids **91**, 170 (1987).

[55] T. Uchino, M. Takahashi, and T. Yoko, Phys. Rev. Lett. **86**, 1777 (2001).

[56] P. E. Blöchl, Phys. Rev. B **62**, 6158 (2000).

[57] K. L. Yip and W. B. Fowler, Phys. Rev. B **11**, 2327 (1974).

[58] N. Itoh and A. M. Stoneham, *Materials Modification by Electronic Excitation* (Cambridge University Press, Cambridge, 2001).

[59] A. D. Becke, J. Chem. Phys. **98**, 5648 (1993).

[60] C. Lee, W. Yang, and R. G. Parr, Phys. Rev. B **37**, 785 (1988).

[61] Y. Zhang and W. Yang, J. Chem. Phys. **109**, 2604 (1998).

[62] J. L. Gavartin, P. V. Sushko, and A. L. Shluger, Phys. Rev. B **67**, 035108 (2003).